HHS Public Access

Author manuscript

Nat Neurosci. Author manuscript; available in PMC 2019 August 25.

Published in final edited form as:

Nat Neurosci. 2019 April ; 22(4): 565–575. doi:10.1038/s41593-019-0337-z.

Divergent medial amygdala projections regulate approach-avoidance conflict behavior

Samara M. Miller[1], **Daniele Marcotulli**[1,2], **Angela Shen**[3], and **Larry S. Zweifel**[1,4]

[1.]Department of Pharmacology, University of Washington, Seattle, WA 98185.

[2.]Department of Experimental and Clinical Medicine, Università Politecnica delle Marche, Ancona, Italy.

[3.]Department of Anthropology, University of Washington, Seattle, WA 98185.

[4.]Department of Psychiatry, University of Washington, Seattle, WA 98185

Abstract

Avoidance of innate threats is often conflicted by motivations to engage in exploratory approach behavior. The neural pathways that mediate this approach-avoidance conflict are not well resolved. Here, we isolated a population of dopamine D1 receptor (D1R) expressing neurons within the posteroventral region of the medial amygdala (MeApv) in mice that are activated either during approach or during avoidance of an innate threat stimulus. Distinct subpopulations of MeApv-D1R neurons differentially innervate the ventromedial hypothalamus (VMH) and bed nucleus of the stria terminalis (BNST) and these projections have opposing effects on investigation or avoidance of threatening stimuli. These projections are potently modulated through opposite actions of D1R signaling that bias approach behavior. These data demonstrate divergent pathways in the MeApv that can be differentially weighted towards exploration or evasion of threats.

Introduction

Animals across all levels of complexity possess approach mechanisms that evoke social and exploratory behavior, and avoidance behaviors that evoke withdrawal and flight[1]. In order to maximize gains, animals will engage in risky exploratory behavior, ignoring signs of potential threat, to exploit resources in their environment. Animals exposed to competing environmental cues must negotiate between mutually incompatible behaviors, such as

Correspondence: larryz@uw.edu.

Author Contributions

S.M.M. and L.S.Z designed experiments. S.M.M. and L.S.Z wrote the manuscript. S.M.M. performed all viral injection surgeries, behavior, and slice electrophysiology. D.M. analyzed all calcium imaging data. Behavioral analysis and histology was performed by S.M.M. and A.S. L.S.Z purified all viral vectors.

Data and Code Availability

Datasets supporting the findings in this study and custom codes used for imaging analysis are available from the corresponding author upon request.

Competing financial interests

The authors declare no competing financial interests.

feeding, reproduction, flight or defense. In some contexts, threatening stimuli, such as predators or aggressive conspecifics, will suppress appetitive behavior, such as reproduction[2]. Conversely, hunger and food seeking will override defensive behaviors[3].

Defensive responses can be adaptive depending on the fed state of an animal and evidence suggests that these adaptations specifically involve neurons in sub-regions of the medial amygdala (MeA)[4]. Thus, animals require integrated circuits to generate gradients of defensive responses appropriate to the contextual threat, and approach responses proportional to potential gains. A major conflicting drive of innate avoidance is an inherent motivation to approach and explore the unknown. In the classical sense of approach-avoidance conflict, exploratory drive is an essential feature of maximizing an animal's ability to thrive, whereas avoidance is essential for survival[1].

Early lesion and electrical stimulation studies have provided intriguing insight into potential loci of approach-avoidance interactions. In rats, electrolytic lesion of the corticomedial amygdala, which encompassed the MeA, elicited a reduction in freezing behavior and an increase in exploratory interactions with a live cat, a natural predator of the rat[5]. Similarly, more restricted excitotoxic lesion of the MeA greatly reduces defensive behavior in rats during exposure to a live cat and increases exploratory locomotion[6]. These finding supports the idea that innate approach of the unfamiliar cat is actively suppressed by the innate avoidance impulse. In contrast to lesions, electrical stimulation of subcortical brain regions can elicit either approach, avoidance, or in some cases ambivalent responses[7]. Intriguingly, the regions that produced these ambivalent responses are innervated by the MeA, including the bed nucleus of the stria terminalis (BNST) and the ventromedial hypothalamus (VMH).

In addition to lesion studies, activity mapping using the immediate-early gene Fos has strongly implicated the MeApv in the processing of innate threat cues[2,6,8,9]. Retrograde tracing and Fos expression analysis revealed that MeApv neurons that were activated by threat stimuli projected to hypothalamic nuclei are implicated in both appetitive (reproduction) and aversive behaviors[2]. In contrast, MeApv neurons activated by reproductive stimuli did not project to these regions[2]. Based on these observations, it was hypothesized that the MeA-hypothalamic pathway may be an important "gate" between conflicting appetitive behavior and threatening stimuli, either through interneurons within the VMH or through indirect modulation by the BNST[2].

We recently identified the MeA as a brain region activated in response to stimulation of midbrain dopamine neurons[10]. The midbrain dopamine system plays an essential role in reward learning, motivation, fear learning and avoidance of conditioned stimuli[11]. Recent data support a role for dopamine in modulating approach-avoidance conflict. Increasing dopamine activity by lesioning an inhibitory input onto dopamine neurons in the VTA causes animals to display increased approach to a predator odor threat[12]. Additionally, increasing dopamine with the use of monoamine oxidase inhibitors is an effective treatment for specific phobias[13], disorders likely caused by dysfunction in innate fear circuitry[14].

The MeA is considered part of the caudal striatum, or more generally a component of the striatopallidal complex[15,16]. This anatomical association suggests that the MeA may be

functionally involved in dopamine-dependent behaviors. Given the role of the MeA in regulating innate defensive responses[17], along with the observation that dopamine neurons of the midbrain are connected to this striatopallidal-like structure[10], we hypothesized that dopamine receptive neurons in this region would likely contribute to innate approach and avoidance behavior. We identified dopamine receptive neurons in the MeA that express D1R and are strongly biased in their localization to the MeApv. Using viral tracing methods, calcium imaging, and optogenetic/pharmacological manipulations, we find that MeApv D1R neurons segregate into distinct populations that regulate either approach or avoidance of innate threat stimuli. These populations regulate approach and avoidance behaviors through two separate projections, one largely inhibitory projection to the BNST, and one largely excitatory projection to the dorsomedial VMH (VMHdm)

Results

Identification of dopamine receptive neurons in the MeApv

Using cell-type specific expression of the stimulatory DREADD receptor HM3Dq in dopamine neurons of the ventral midbrain, we recently demonstrated that activation of dopamine neurons induces Fos in the MeA[10]. To confirm the presence of dopamine receptive neurons in this region, we searched the Allen Institute for Brain Science Mouse Brain *in situ* hybridization atlas[18] for dopamine receptor expression in the amygdala. Within the MeA, *Drd1* was expressed prominently in the MEApv; high levels of *Drd1* were also observed in the intercalated cell clusters, and to a lesser extent in the BLA and CeA. In contrast, we did not observe appreciable levels of expression of *Drd2, 3, 4, or 5* in the MeA, though varying degrees of expression of these genes were seen in other amygdala nuclei. To confirm the presence of *Drd1*-expressing neurons in the MeA, we crossed $Drd1^{Cre/+}$ (D1R-Cre[19]) mice to the fluorescent reporter line Ai14[20] (floxed:stop tdTomato). Fluorescently labeled neurons were detected in the MeApv, and we observed a significantly biased distribution of tdTomato positive neurons in the MeApv as compared to the posterodorsal MeA (MeApd) (Figure 1a–b).

Consistent with innervation of the MeA by dopamine producing neurons, injection of a Cre-dependent adeno-associated virus (AAV1) containing an expression cassette for the fluorescent reporter synaptophysin-GFP (AAV1-FLEX-Syn-GFP) into the ventral tegmental area/substantia nigra pars compacta (VTA/SNc) of mice expressing Cre recombinase from the endogenous dopamine transporter locus, $Slc6a3^{Cre/+}$ (DAT-Cre[21]) revealed a significant bias of Syn-GFP puncta localized to the MeApv compared to the MeApd (Figure 1c). To test for functional D1R signaling in the MeApv, we injected the D1R agonist SKF-81,297 intraperitoneally (7.5mg/kg) and immunostained for Fos protein. We observed robust Fos in the MeA relative to saline controls, and higher Fos in the MeApv relative to the MeApd (Figure 1d).

To further establish the localization of D1R within the MeA and its relationship to other previously identified genetic markers within this region[2,4,22], we performed fluorescence in situ hybridization analysis for mRNA localization using RNAscope[23]. Consistent with the localization of MeA-D1R neurons observed in the D1R-Cre::Ai14 line and Fos localization following SKF-81,297 administration, we observed a strongly biased expression of *Drd1* in

the MeApv compared to the MeApd (Figure 1e–g). In contrast to *Drd1*, *Lhx6* expression was biased towards the MeApd (Figure 1e) and *Cyp19a1* (aromatase) did not show a differential expression pattern (Figure 1f). Similar to *Drd1*, *Npy1r* was differentially localized with biased expression in the MeApv (Figure 1g). *Npy1r* showed more overlap with *Drd1* in the MeApv than did either *Lhx6* or *Cyp19a1* (Figure 1e–g; 40.1 ± 3.5, 6.1 ± 1.2, and 23.6 ± 3.2% respectively, One-way ANOVA $P<0.0001$).

MeApv-D1R neurons are activated during approach and avoidance

It has been shown that exposure to innate threat stimuli, such as predator odorants and intruder conspecifics, induces Fos expression in the MeApv[6,24,25]. To determine if MeApv-D1R neurons are specifically activated by innate threat stimuli, we virally labelled these neurons with GFP and exposed mice to a variety of multi-sensory threats (Supplementary Figure 1a). These threats included cat urine, previously shown to elicit physiological fear responses in mice[26] (predator odor, PO), an intruder conspecific that evokes olfactory, auditory, and visual social fear[17,27] (conspecific intruder, CI), and a large robotic bug (robobug, RB) that simulates an auditory/visual predatory threat[28]. We observed increased Fos in a significant proportion of MeApv-D1R neurons in response to these cues that was equivalent across stimuli (Supplementary Figure 1b–e).

To attain better temporal resolution of the activity of MeApv-D1R neurons, we performed calcium imaging[29] of the MeApv-D1R neurons during exposure to robobug, predator odorant and conspecific bedding (soiled bedding was used as a proxy for a conspecific intruder to prevent damaging imaging equipment in case of aggression or fighting). GCaMP6m[30] was conditionally expressed in the MeApv of D1R-Cre mice by intracranial injection of AAV1-FLEX-GCaMP6m (Supplementary Figure 2a and b). Calcium signals were acquired in response to the distinct stimuli for a period of six minutes following a two minute baseline period (Figure 2a). In all assays, mice were given access to a hidebox for avoidance (Figure 2a). To determine whether MeApv-D1R neurons are active during approach or avoidance, we analyzed isolated cells (Figure 2b) in four mice (2 male, 2 female). Exploratory and avoidance epochs were highly variable in response to the predator odor and robobug (Supplementary Table 1; Supplementary Figure 2c–f), and mice spent the majority of time in the hidebox in response to both stimuli (Supplementary Figure 2g).

To establish whether calcium signals were selective for designated behavioral epoch, activity of each cell was shuffled to generate a null distribution. Cells with calcium signals during behavioral epochs with unshuffled data and complete inactivity during these epochs with shuffled data were categorized as selective. The inactivity threshold was established through iterative multiples of the mean activity until a threshold in which no cell was categorized as selective during an epoch using shuffled data across all mice and all sessions. During exposure to the robobug and predator odor, we observed an increase in calcium signals in a subpopulation of neurons immediately prior to investigation (approach, Figure 2b–j) and a largely non-overlapping population that became active during avoidance in the hidebox (Figure 2b–j; Supplementary Figure 2h–k). Probability of distribution analyses of responsive cells confirmed peak activity centered proximal to the designated event (Figure 2e–f). We also observed smaller subsets of neurons activated directly following initiation of

investigations or activated just prior to entry to the hidebox area (Figure 2 e, f, h, and i). Cells responsive during the hidebox or investigation periods in response to either robobug or predator odor were largely non-overlapping (Supplementary Figure 2m–n, Supplemental Table 2) indicating a segregation of processing for these distinct stimuli.

In response to conspecific odorants, we observed highly variably behavioral responses (Supplementary Figure 3a–f, Supplementary table 1.). Although mice were exposed to soiled bedding from both male and female conspecifics, we generally observed calcium signals during investigation of all bedding in all mice (Supplementary Figure 3a). Preliminary data suggests subtle differences in the selectivity of MeApv-D1R neurons in male and females, and that female and male odorant-responsive neurons were largely non-overlapping in both male and female mice (Supplementary Table 2). However, given the low sample size for each sex (n=2 males, 2 females), we cannot make any conclusions about sexually dimorphic encoding of social information by MeApv-D1R neurons.

MeApv-D1R neurons differentially innervate the BNST and VMH

To establish the downstream connections of MeApv-D1R neurons, we bilaterally injected AAV-FLEX-Syn-GFP into the MeApv of D1R-Cre mice. Consistent with previous reports of MeApv projections[31], we observed dense GFP-positive puncta in the VMH and BNST (Figure 3a), with a significant bias toward a higher density projection to the BNST (integrated pixel density, BNST = 655.5 ± 105.4 versus VMH = 320.5 ± 105.9, P = 0.039, N = 3 mice). Analysis of the anatomical distribution of MeApv-D1R fibers revealed projections localized most prominently to the transverse (tr) nucleus of the BNST (Figure 3b) and the dorsal medial (dm) subdivision of the VMH (Figure 3c), consistent with previous anatomical analysis of MeApv projections[15,31,32]. To determine whether projections from the MeApv to the VMH and BNST represent collaterals or independent projections, we co-injected retrogradely transported red fluorescent beads (RetroBeads) into the VMH and green RetroBeads into the BNST of wild-type mice (Figure 3d). Both red and green RetroBeads were observed in the MeApv, with a stronger labeling of BNST projection neurons. We observed very few neurons with overlapping red and green fluorescent beads (Figure 3d).

To characterize the synaptic connectivity of MeApv-D1R neuron projections to the VMHdm and BNST, we transduced MEApv-D1R neurons with a conditional channelrhodopsin[33] (ChR2)-expressing virus (AAV1-FLEX-ChR2-mCherry). Following viral expression, we photostimulated MEApv-D1R terminals and performed whole-cell recordings in the BNST and the VMH (Figure 4e–f, Supplementary Figure 4a–b). In the BNST, 15 out of 31 cells displayed a light-evoked inhibitory postsynaptic current (IPSC) that was blocked by the $GABA_A$ receptor antagonist picrotoxin (Figure 3e). A smaller proportion of cells showed short latency excitation (3 of 31). In a subset of cells (4 out of 31), we observed delayed inhibitory input that was blocked by CNQX suggesting feed forward inhibition (Supplementary Figure 4c). In the VMH, 9 out of 15 cells displayed a light-evoked excitatory postsynaptic current (EPSC) that was blocked by the AMPA glutamate receptor antagonist CNQX (Figure 3f). We also observed one cell with delayed inhibition and one cell with delayed excitation, consistent with feedforward synaptic transmission. These data

demonstrate an excitatory MeApv projection to the VMH and predominantly inhibitory projection to the BNST that is consistent with distinct projection populations of MeApv-D1R neurons.

VMH and BNST-projecting MeApv-D1R neurons differentially regulate innate fear

To determine whether BNST and VMH projecting MeApv neurons are activated by threat stimuli, we injected RetroBeads into either the BNST or VMH and exposed mice to predator odorant, robobug or the conspecific intruder assay (Supplementary Figure 5a). Consistent with our projection mapping, we observed a larger number of cells projecting to the BNST than to the VMH (Supplementary Figure 5b). BNST and VMH projecting MeApv neurons were both activated by innate threat stimuli in all assays (Supplementary Figure 5c); however, a significantly larger proportion of VMH projecting MeApv neurons compared to BNST-projecting MeApv neurons were activated by predator odor and robobug, but not to an intruder conspecific (Supplementary Figure 5d and e).

To examine the role of distinct MeApv-D1R pathways in regulating avoidance and approach, we optogenetically stimulated MeApv-D1R→VMH and MeApv-D1R→BNST terminals in freely behaving mice exposed to threat stimuli (10Hz, 3 sec on/3 sec off; Figure 4a and b). MeApv-D1R neurons were unilaterally transduced with AAV1-FLEX-ChR2-mCherry or AAV1-FLEX-mCherry (control) in D1R-Cre mice, and an optic fiber was implanted directly over the VMH or the BNST (Figure 4a; Supplementary Figure 6a–c). Direct stimulation of MeApv-D1R→VMH projections enhanced defensive avoidance behaviors (i.e. increased time spent in hidebox and decreased exploration of the threat) in response to a predator odor (Figure 4c) and robobug (Figure 4d). In contrast, MeApv-D1R→BNST stimulation decreased avoidance of these threats and increased exploratory investigations (Figure 4c–d).

In response to a conspecific threat in the resident-intruder assay, male mice will display territorial aggression towards an intruder[34]. To assess whether MeApv-D1R projections to the VMH or BNST influence this behavior, we stimulated these projections during a resident-intruder assay. MeApv-D1R→VMH stimulated mice showed significantly increased grooming of the male conspecific intruder and less aggression (Figure 4e), whereas MeApv-D1R→BNST stimulated mice showed a significantly increased aggression phenotype (Figure 5e). Across the groups, we did not observe significant differences in total time spent investigating the intruder (Figure 4e).

To establish whether MeApv-D1R→VMH or MeApv-D1R→BNST connections are inherently rewarding or aversive, we performed a real-time place preference (RTPP) assay during terminal stimulation. We observed an increased avoidance of the light-paired chamber in MeApv-D1R→VMH stimulated mice relative to the unpaired side (Supplementary Figure 7a–b). MeApv-D1R→VMH stimulated mice exhibited a small but significant reduction in distance traveled compared to MeApv-D1R→BNST stimulated mice, but not compared to controls (Supplementary Figure 7c). In contrast, MeApv-D1R→BNST stimulation had no significant effect on RTPP behavior (Supplementary Figure 7a–b).

Our connectivity analysis indicates that MeApv-D1R neurons are heterogeneous, and dominantly release glutamate at VMH terminals and GABA at BNST terminals. We also find that these pathways together regulate innate defensive behaviors bidirectionally. To determine whether these projections are truly functionally opposed, or whether one can dominate the other, we optogenetically stimulated MeApv-D1R cell bodies (Supplementary Figure 8a) in the presence of innate threat stimuli. Similar to MeApv-D1R→BNST terminal stimulation, collective stimulation of MeApv-D1R cell bodies reduced fear in the predator odor and robobug assay, and enhanced aggression in the resident-intruder assay (Supplementary Figure 8b–d). MeApv-D1R cell body stimulation also did not induce a change in behavior in the RTPP assay (Supplementary Figure 8e). These data suggest that when co-activated, the BNST pathway overrides the VMH projection to bias behavior towards approach.

To establish whether inhibiting these pathways alters approach and avoidance behaviors related to threats, we performed projection-specific inhibition of MeA-D1R→BNST and MeA-D1R→VMH pathways using the inhibitory opsin Jaws[35]. The retrograde transducing AAV, AAV2-retro[36] containing a Cre-dependent expression cassette for Jaws was injected into either the VMH or BNST of D1R-Cre mice (Figure 5a and b; Supplementary Figure 9a–d). Cells bodies projecting to the VMH or BNST were inhibited during each assay with red light (1s on with a 1s ramp-down, 2s off) delivered to the MeApv. Consistent with activation of the VMH pathway eliciting increased avoidance behavior, inhibition of this projection reduced avoidance behavior in the predator odorant assay (Figure 5c) and the robobug assay (Figure 5d). Inhibition of the VMH projection neurons did not alter grooming behavior, but significantly enhanced aggression (Figure 5e). In contrast to inhibiting the VMH projection population, inhibition of the BNST projections did not significantly alter these behaviors (Figure 5c–e). Thus, under these conditions the MeApv-D1R→VMH pathway appears to be predominantly regulating avoidance behavior.

D1R signaling biases activation of the MeA→BNST approach pathway

It is well established that transient elevated levels of dopamine release in the striatum promote conditioned approach to rewarding stimuli that is mediated in part by dopamine signaling through D1R[37] to enhance incentive motivational drive[38]. To establish whether D1R signaling modulates the excitability of MeApv projections to the VMH or BNST, we recorded MeApv-D1R neurons in an acute brain slice preparation. MeApv-D1R neurons were identified by expression of tdTomato using the D1R-Cre::Ai14 line. Projection specificity was determined by injection of green Retrobeads into either the BNST or VMH (Figure 6a and b). Excitability was measured as the number of action potentials elicited by increasing current injection (10 pA steps, 10 to 60 pA) in the absence (ACSF) or presence of the D1R agonist SKF 81,297 (10 μM). As expected, SKF bath application increased the excitability of BNST projecting neurons (9 of 16 cells, Figure 7a, c-e). Paradoxically, SKF application reduced the excitability of VMH projecting neurons (8 of 14 cells, Figure 6b–e) that was associated with a hyperpolarization of the resting membrane potential (Figure 6f).

To determine whether increasing dopamine D1R signaling on MeApv-D1R alters defensive behavior, we bilaterally infused the D1R agonist SKF 81,297(0.1 μg or 1μg/0.5 μl per side)

directly into the MeApv of wild type mice through stereotaxically implanted cannula (Figure 6g; Supplementary Figure 10). Infusion of SKF 81,297 suppressed fear responses following exposure to innate threat stimuli and enhanced approach and aggression in a dose-dependent manner (Figure 6h–j). SKF 81,297 infusion did not alter locomotor behavior in these assays (Supplementary Figure 10). Taken together, these data support a role for MePV-D1R neurons in the modulation of innate fear behavior and demonstrate that the MeA-D1R→VMH and MeA-D1R→BNST pathways are not equivalent in their opposition, but rather can be biased toward approach. We propose that during periods of high incentive motivation, such as during the drive to acquire rewards, behavior is biased towards approach in the face of potential danger that is predicated by state-dependent levels of dopamine in the amygdala (Figure 6k and l).

Discussion

We find that MeApv-D1R neurons can be parsed into inhibitory and excitatory projections to the BNST and VMH, respectively, which differentially regulate defensive behavior. Our data are consistent with the striatopallidal-like designation of the MeA and its potential as a caudal extension of the striatum, though there are some clear distinctions. Like the striatum, the MeA contains dopamine-receptive neurons and appears to possess a type of direct and indirect pathway. First, MeApv-D1R neurons send a direct excitatory projection to the VMHdm to regulate innate defensive behaviors. Second, MeApv-D1R neurons send an inhibitory projection to the BNST which may serve as an indirect pathway. Consistent with previous anatomical analysis of MeApv projections, MeApv neurons preferentially innervate the BNSTtr and to a lesser extent the BNSTif, both of which project to the defensive nuclei in the hypothalamus; notably the BNSTif projects to the VMHdm[39]. The manner in which GABAergic projections from the MeApv-D1R neurons to the BNST suppress defensive behavior remains unclear. One possibility is that these projections would inhibit intra-BNST GABAergic interneurons to disinhibit GABAergic outputs to the hypothalamus. Alternatively, inhibitory MeApv-D1R→BNST projections could inhibit GABAergic projections to appetitive behavioral centers, thus providing a disinhibitory gate as proposed previously[2]. Interestingly, the BNSTtr has also been shown to send a significant projection to the VTA[39] and both the BNSTif and BNSTtr project back to the MeA[39], providing multiple potential feedback loops.

In contrast to the striatum, in which D2Rs inhibit the indirect pathway and D1Rs stimulate the direct pathway, we find D1R signaling enhances the activity of the putative BNST indirect pathway and inhibits the putative VMH direct pathway. Though paradoxical, the inhibition of VMH projection neurons by the D1R is not unprecedented. Notably, D1R signaling has been shown to inhibit neurons within the amygdala in a cell-autonomous manner[40]. Future investigations to determine the cell-autonomous effects of D1R activation in MeApv-D1R neurons will provide additional insight into the organization of this system and the role of dopamine in modulating circuit function.

Dopamine has been highly implicated in incentive motivational processes underlying reward seeking and conditioned fear[41,42], but whether dopamine is a key modulator of circuits underlying approach and avoidance conflict has not been established. Here we demonstrate a

role for dopamine in innate fear behavior through the modulation of dopamine D1R signaling in the MeApv. Specifically, we show that increasing D1R signaling onto MeApv-D1R neurons increases approach behavior, likely through the simultaneous suppression of the VMH pathway and activation of the BNST pathway. This finding is consistent with previous studies demonstrating that a significant fraction of dopamine neurons are inhibited by aversive stimuli and activated by appetitive stimuli[41]. Under these conditions dopamine levels would be low during threat encounters and high during increased incentive motivation. Thus, when an animal is threatened, reduced dopamine would promote the activation of the VMH avoidance pathway, and under increased appetitive motivational states elevated dopamine levels would promote activation of approach pathways and suppression of avoidance pathways. Interestingly, it has recently been shown that activation of distinct inhibitory subpopulations within the laterodorsal tegmentum (LDT) oppositely regulate olfactory cue-induced freezing to an innate threat[43]. Given that the LDT is a potent regulator of the midbrain dopamine system this represents a putative mechanism for differential regulation of MeApv dopamine levels through inhibitory/disinhibitory projections of the LDT.

MeApv-D1R neurons that evoke GABA-mediated inhibition of the BNST elicit approach behavior to threat stimuli, including aggression towards conspecifics. Conversely, MeApv-D1R neurons that evoke glutamatergic excitation of the VMHdm enhance avoidance of threatening stimuli, and grooming of conspecifics. Consistent with our observation, stimulation of the VMHdm enhances innate fear behaviors such as hiding and freezing[44]. We find that inhibition of the MeApv-D1R→VMH pathway suppresses defensive behavior, consistent with these neurons directly influencing defensive behavior. We did not find an effect of inhibiting the BNST pathway during exposure to innate threats. One potential explanation for this observation is that if the BNST serves as a gate to permit exploratory behavior, and the internal drive is sufficiently low, closing this gate further may have a minimal effect.

The amygdala is composed of multiple distinct and interconnected nuclei involved in threat detection[17], as well as hedonic and consummatory processes[45,46]. The MeApd and MeApv are thought to be differentially involved in defensive responses to either conspecifics or predators[17,24]. In rodents, the MeApd is robustly activated by aggressive conspecifics, while the MeApv is strongly activated by a live cat or its odor[2,6,8,9,24]. Anterograde tracing studies have demonstrated that the MeApd projects to regions implicated in reproduction and conspecific responsive behavior, including the ventrolateral VMH (VMHvl)[25,31]. In contrast, the MeApv projects to distinct hypothalamic nuclei involved in predator-responsive and general avoidance behavior, including the VMHdm[31,47]; though projections to the VMHvl have also been reported[2]. Activation of independent pathways from the VMHdm to either the periaqueductal gray or the anterior hypothalamic nucleus can evoke either freezing or avoidance in response to threats, respectively[47]. Based on previous hypotheses that conspecific and predatory threats are differentially regulated by the MeApd and MeApv[17,44], respectively, we were surprised to find that projection-specific pathways from the MeApv differentially regulated conspecific male aggression. However, our data are consistent with previous reports showing Fos induction in the MeApv in response to a male conspecific[25].

Further supporting the diverse functions of MeApv-D1R neurons, our *in vivo* imaging data demonstrates that these cells respond to a variety of threatening and appetitive stimuli. Subsets of neurons were activated during the hidebox period and largely non-overlapping neurons were activated proximal to the investigation periods. These data support the hypothesis that distinct populations regulate approach and avoidance behavior. Cells activated proximal to investigation were largely activated leading up to the investigation, but were largely silent once the active investigation was initiated. Based on this observation we suggest that these neurons play an important role in approach. Cells activated during the hidebox period showed largely constrained activity that peaked shortly after entry into the hidebox. Although this activity is consistent with the avoidance of the stimulus it remains possible that these cells represent a type of safety signal engaged once an escape has been successfully completed. In addition to responding to threat stimuli, MeApv-D1R neurons were also activated by conspecific odorants, and projection-specific activation of MeApv-D1R neurons significantly impacted male-male interactions. Additional calcium imaging studies with larger sample sizes are required to assess the selectivity of MeApv-D1R neurons in male and female mice to both same- and opposite-sex conspecifics. Sex-specific social processing within the MeA likely gates state-dependent behaviors to differentially drive aggression versus investigation in particular contexts[2,17]. Future investigations are needed to understand how MeApv-D1R neurons regulate male-female and female-female social behaviors and this type of information processing.

Aggressive behavior towards intruder conspecifics was once viewed as a purely defensive response; however, recent studies have revealed that aggression in rodents generates a conditioned place preference and increases nucleus accumbens dopamine levels[48,49]. Specifically, microdialysis experiments in the nucleus accumbens in aggressive males revealed that DA levels increase prior to an anticipated fight and can remain elevated during and after a single fight[49]. Additionally, local dopamine receptor blockade in the nucleus accumbens decreases aggression motivated operant responding[50]. Our findings that activation of the MeApv-D1R→BNST pathway increases aggression may reflect a parallel or integrated mechanism by which increased amygdalar dopamine generates a motivational state to drive aggression. However, we cannot exclude the possibility that the small number of D1R neurons localized to the MeApd is regulating the observed aggressive behavior.

In conclusion, our data demonstrate that distinct approach and avoidance pathways exist within the MeApv. These two pathways segregate based on distinct projection patterns and neurotransmitter phenotype, but represent interspersed ensembles at the level of the MeA. The identification of a brain locus underlying approach-avoidance conflict permits further resolution of upstream and downstream pathways critical for resolving these behavioral conflicts.

Methods

Animals

All experiments were approved in accordance with the guidelines of the Institutional Animal Care and Use Committee of the University of Washington. *Drd1a*$^{Cre/+}$ mice and *Slc6a3*$^{Cre/+}$ (DAT-Cre) mice have been characterized previously[19,51]. The Ai14 Cre-dependent reporter

strain, *Rosa26Sor*$^{fs\text{-}Tdt}$, was purchased from Jackson Laboratories (stock #007914). Approximately equal numbers of male and female mice were used for all experiments, with the exception of the resident-intruder assay, in which only male mice were used. Mice were housed on a 12-hr light cycle and given *ad libitum* access to food and water. Behavioral mice were 8 weeks or older, and mice used for slice electrophysiology were 5–8 weeks old. Mice were group housed, with the exception of resident male mice which were singly housed 2–3 weeks prior to the resident-intruder assay. Mice were bred onto a C57BL/6J background, and mice used for social interaction assays were wild-type C57BL/6J. Mice were assigned randomly to control or experimental groups, and experimenters were blinded during data analysis.

Viruses and neuronal tracers

All viruses were produced in house with titers of 1–3 × 10^{12} particles per mL as described[52]. RetroBeads™ were obtained from Lumafluor and injected with a Hamilton syringe (0.5μl/hemisphere). In accordance with manufacturers protocol, red Retrobeads™ were injected at a dilution of 1:4 and green Retrobeads™ were injected undiluted.

Surgery

Mice were anesthetized with isoflurane and secured on a stereotaxic alignment device (David Kopf instruments) before injection. Body temperature was maintained with a heating pad during surgery and 1.5–2% isoflurane was delivered continuously through a nose port. Injection coordinates were as follows from bregma in mm: MeA_{PV}, A-P: −1.5; M-L: ±2.5, D-V: −5.6; BNST, A-P: 0.2, M-L: ±1.25, D-V: −4.25; VMH_{DM}, A-P: 1.15, M-L: ±0.5, D-V: −5.5; VTA, A-P: −3.25, M-L: ±0.5, D-V: −4.5. For *in vivo* ChR2 and Jaws experiments, fiber optic cannulae were manufactured in house as described[53]. For ChR2 experiments, optic fibers were implanted unilaterally 0.5mm above the coordinates listed for viral injection. For Jaws experiments, optic fibers were implanted bilaterally 0.5mm above the coordinates for the MeApv. For microinfusion experiments, cannulae were implanted lateral to MeA_{PV} at M-L: ±2.6mm from bregma. Behavioral testing and slice electrophysiology experiments began following a minimum of a 2 week surgical recovery period, with the exception of RetroBead and microinfusion surgeries in which recovery was only 1 week. Following behavioral testing, injection sites and fiber implant placements were confirmed using immunohistochemistry on collected brain tissue sections. Mice with mistargeted injections or implants were excluded from this study.

Calcium imaging surgeries were performed as described previously[54]. *Drd1a*$^{Cre/+}$ mice were injected with AAV1-FLEX-GCaMP6m and AAV1-FLEX-HM3-mCherry using the stereotaxic protocol described above. Three weeks later mice were implanted with a microendoscope lens (length: 7.3mm, diameter: 0.6mm; Inscopix). Animals were injected with 1mg/kg CNO at the start of the surgery to visualize neuronal activity during implantation. The lens was implanted ~200–300 μm above the viral injection site. One week after the lens implant, mice were anaesthetized so that a baseplate (Inscopix) could be implanted over the lens to serve as an interface between the miniature microscope and the lens during experiments. A dummy miniature microscope (Inscopix) was used to habituate

animals for ~5 days prior to any behavioral experiments. Only animals with successful lens implants were used for this study.

Immunohistochemistry

Primary antibodies were against GFP (mouse, 1:1000, Invitrogen A11120[55]; or rabbit, 1:1000, Invitrogen A11122)[56], c-Fos (rabbit 1:2000, Milipore ABE457)[57], or TH (mouse, 1:1000, Milipore MAB318)[58]. Secondary antibodies were conjugated to DyLight488 or CY3 (1:250, Jackson Immunolabs #711-165-153, 715-165-150, 711-545-152, 715-545-150). All staining was done on free-floating 30 μm sections (overnight primary incubations at 4°C).

Single-molecule fluorescence in situ hybridization

We performed single-molecule fluorescence in situ hybridization using RNAscope fluorescence detection assays and probes (ACDbio RNAscope® Probe-mm-*Cyp19a1* #430821; RNAscope® Probe-mm-*Drd1* #463851; RNAscope® Probe-mm-*Npy1R* #427021; RNAscope® Probe-mm-*Lhx6* #422791) in 8–9 week old mice according to the manufacturer's protocols. Brains were flash-frozen in 2-methylbutane and the medial amygdala was sectioned at 10 μm along the rostral-caudal axis. Tissue was used within one week after cryosectioning.

Electrophysiology

Coronal brain slices (250 μm) were prepared from mice aged 5–8 weeks old in an ice slush solution containing (in mM): 92 NMDG, 2.5 KCl, 1.25 NaH_2PO_4, 30 $NaHCO_3$, 20 HEPES, 25 glucose, 2 thiouria, 5 Na-ascorbate, 3 Na-pyruvate, 0.5 $CaCl_2$, 10 $MgSO_4$, pH 7.3–7.4[59]. Slices recovered for ≤12 minutes in the same solution at 32° before recovering for an additional 45 minutes at room temperature in a solution containing (in mM): 92 NaCl, 2.5 KCl, 1.25 NaH_2PO_4, 30 $NaHCO_3$, 20 HEPES, 25 glucose, 2 thiouria, 5 Na-ascorbate, 3 Na-pyruvate, 2 $CaCl_2$, 2 $MgSO_4$. All solutions were continually bubbled with O_2/CO_2, and all recordings were made at 32° in aCSF (in mM: 126 NaCl, 2.5 KCl, 1.25 NaH_2PO_4, 1.2 $MgCl_2$, 10 glucose, 25 $NaHCO_3$, 2 $CaCl_2$) continuously perfused over slices at a rate of ~2 ml/min. Whole-cell patch clamp recordings were made using Axopatch 700B amplifier (Molecular Devices) with filtering at 1 KHz using 4–6 MΩ electrodes filled with an internal solution containing (in mM): 130 K-gluconate, 10 HEPES, 5 NaCl, 1 EGTA, 5 Mg-ATP, 0.5 Na-GTP, pH 7.3, 280 mOsm. Light evoked synaptic transmission was induced with 5 ms light pulses delivered at a rate of 0.1 Hz from an optic fiber placed directly in the bath. To measure excitatory responses, cells were held in voltage-clamp mode at −60 mV. For inhibitory evoked responses, cells were held in voltage-clamp mode at 0 mV. CNQX (10 μM) and picrotoxin (100 nM) were bath applied to block excitatory and inhibitory responses, respectively. Responses were characterized as delayed if they were between 6–15ms after termination of blue light. SKF 81,297 (10 μM) was perfused over the slices for approximately 2–3 minutes before recording its effect. Excitability was measured as the number of action potentials in response to current injections of varying amplitudes before and after drug application.

Fos Induction

Experimental mice were singly housed and placed into the empty behavioral arena each day for 3 days prior to the experiment in order to acclimate them to handling and context. On test days, mice were exposed to single threat stimuli for 3–5 minutes. Mice were sacrificed 90 minutes following exposure to stimuli.

Fos-positive neurons were identified and counted using ImageJ software. Virally transduced D1R neurons and Fos-positive D1R neurons were counted by hand by an experienced investigator blind to condition.

Mapping analysis

A conditional virus packaged with synaptophysin tagged to GFP (AAV1-FLEX-synaptoGFP[60]) was used to characterize downstream projections of MeApv-D1R neurons. Pixel density in downstream target areas was quantified using ImageJ software. The "Measure" feature of ImageJ was used to quantify the integrated pixel density within a standardized region of interest (ROI) drawn based on previous classifications from the Allen Brain Atlas and other literature[15].

Behavior

For all ChR2 behavioral experiments, blue light stimulation parameters were 10 Hz, 5 ms, 3 seconds on, 3 seconds off. For all Jaws behavioral experiments, red light stimulation parameters were a 2 second pulse with a 1 second ramp down (to prevent rebound excitation), and 1 second off. Experiments were conducted during the light cycle. Animals from each cohort were exposed to all of the following behavioral paradigms in the same order with at least one week of separation in between each. Only male mice from each cohort were tested in the resident-intruder assay. Unless otherwise indicated, all behavioral videos were scored using Ethovision (XT10).

Predator Odor: For the predator odor assay, mice were habituated for 3–4 days to a behavioral chamber with an odorant dish filled with clean cat litter and a hide box on the opposite side of the chamber. On the test day, mice were placed in the chamber for a 5 minute habituation period with an empty odorant dish, followed by a 5 minute test period with blue light stimulation in which the mice were exposed to an odorant dish filled with cat litter saturated in cat urine. Behaviors scored were time spent in hide box, total time investigating the odorant dish, frequency of approaches of the odorant dish and latency to first approach of the odorant dish. Investigation and approach behavior was scored based on an animal's proximity (≤8cm) and orientation to the odorant, which were automatically detected by the Ethovision software.

Robobug: For the robobug assay, mice were placed in a behavioral chamber to which they had been previously habituated. On the test day, mice were placed in the chamber for a 2 minute habituation period followed by a test period with blue light stimulation including a 30 second period in which a robobug apparatus (H: 11cm; W: 11cm; D:13cm; HEXBUG™) was remotely activated. Mice remained in the chamber with the stationary robobug for an additional 2 minutes. Scored behavior included latency to investigate the robobug following

the remote activation period, time spent in hide box, and total time investigating the robobug. As in the predator odor assay, investigation and approach behavior was scored based on animal's proximity (≤8cm) and orientation to the robobug.

Resident-intruder: Resident mice were singly housed for at least two weeks, with a total of 7 days of no cage change, were sexually experienced, and were 3–4 weeks older than intruder mice, which were group housed.[61] Encounters took place during the light cycle. Mice were allowed a 10 minute non-scored habituation period following connection to the fiber optic cable. Intruders were placed into the resident's home cage and the blue light was turned on. Encounters lasted for 20 minutes, and videos were hand scored by an experienced investigator blind to treatment. Behaviors scored were resident-initiated investigation, grooming, and fighting (which included attacking/mounting, high-speed chasing and nudging).

RTPP: Mice were placed in a two-chambered arena with partial walls dividing the two sides that allowed for passage of the fiber optic cable.[62] One side of the area had horizontal black and white stripes, while the other side had vertical stripes. One side was randomly assigned to be paired with blue light stimulation, while the other was unpaired. The assay lasted for 20 minutes.

Calcium imaging studies: A total of 24 mice were injected with AAV1-FLEX-GCaMP6m and AAV1-FLEX-HM3-mCherry. Of those mice, we observed CNO-evoked calcium signals in the MeA in 9 animals that were implanted with GRIN lenses. Of the implanted animals 7 mice showed detectable GCaMP signals with 4 mice displaying detectable signals during multiple behavioral epochs where individual cells could be reliably isolated. All calcium imaging data was collected using 30–50% LED power using a miniature microscope from Inscopix (nVista), and calcium recordings were collected at 5 frames per second and 200-ms exposure time. Behavioral videos and calcium recordings were synchronized using Ethovision (Noldus, XT10). Calcium videos were collected 2 minutes at a time to reduce file size. Behavioral assays were similar to those described above, with the exception of conspecific stimuli. Animals were exposed to an odorant dish containing soiled bedding from cages containing groups of either male or female mice.

Animals were habituated to a dummy miniature microscope in the behavior chamber for 5 days prior to testing. On test day, animals were hooked up to the miniature microscope and placed in the behavior chamber for approximately one hour. To minimize the chance of altering the field of view of the lens, an animal was exposed to all stimuli on the same day with a period of 30–60 minutes in between each assay. All animals were exposed to stimuli in the same order: robobug, predator odor, opposite-sex bedding, same-sex bedding. All behavioral assays for the calcium imaging studies lasted 10 minutes and included a 2 minute pre- and post-test to collect baseline activity of the cells in which there was no stimulus in the behavior chamber. All behavior was hand scored to generate time bins (epochs) designating when an animal approached/investigated or avoided (spent time in the hidebox) the stimulus. Investigation and approach behavior was scored based on an animal's proximity (<~5–10cm) and orientation to the stimulus. The 10 cm designation is one mouse body length in distance. When a mouse displayed a clear orientation towards the stimulus

and was within one body length (10 cm) from the stimulus it was designated as actively approaching. An approach was designated only cif the animal continued to within 5 cm (one half a body length) of the stimulus and maintained an orientation to the stimulus (active investigation range). An additional approach required moving at least 5 cm away from the stimulus and oriented away from the stimulus followed by a reorientation and subsequent approach.

Calcium Imaging Analysis

For each behavioral assay, calcium imaging videos were concatenated and spatially down-sampled by a factor of 2 in Mosaic (Inscopix). To correct for lateral displacements of the brain and prevent motion-induced artifacts, we applied frame-by-frame rigid-body registration using the TurboReg plugin in ImageJ. To prevent the artifactual detection of ROIs along high-contrast borders, we cropped surrounding black borders after registration. After motion correction and cropping of the concatenated videos, neurons were automatically detected using a Constrained Non-Negative Matrix Factorization method for microendoscopic data (CNMF-e)[63,64]. Merging threshold was set to 0.8 for optimal discrimination of temporal and spatial overlap. CNMF-e was also used to extract fluorescence traces of single neurons, and denoise/deconvolve their activity (ΔF). The ΔF was used for all analyses. For each concatenated video, the average ΔF was calculated for every neuron (ROI). Z-scores were calculated using $stats.zscore\ (x\text{-}mean_{ROI\_intensity})/std_{ROI\_intensity}$, with 0 degrees of freedom sourced from the Python SciPy library. Z-scores for individual ROIs were generated using denoised ΔF values within the designated experimental sessions. Field-of view (FOV) images in Figure 2 were generated by applying an FFT bandpass filter to each frame in ImageJ (lower bound 5 pixels, upper bound 50 pixels) and levels were adjusted in Photoshop.

For all assays, cell activity was analyzed from the first 10 seconds of the longest hidebox period. For each animal, only a single hidebox period was analyzed. For robobug and predator odors assay, cell activity was analyzed from ± 5 seconds of investigation periods or series of investigation periods lasting longer than 20 seconds. For each animal, 3–5 investigation periods were analyzed. For conspecific behavioral assays, cell activity was analyzed across all investigation periods. To categorize cells as having calcium signals selective for these epochs, the activity of each cell was shuffled in time to generate a null distribution of Ca^{2+} activity. This null distribution was registered to the behavioral epoch and only cells that showed calcium signals during behavioral epochs with unshuffled data and complete inactivity during these epochs with shuffled data were categorized as selective. The threshold for inactivity was established by generating iterative multiples of the mean activity of each cell during the entire recording session until a threshold in which no cell was categorized as selective during an epoch using shuffled data across all animals and all sessions was obtained. The least common multiple was determined to be 5-times the mean. Thus, cells were only considered selective for given epoch if the average ΔF exceeded this conservative threshold[65]. Heat maps represent z-scores of denoised fluorescent activity ± 15 seconds aligned to an investigation or hidebox event. Events for heat plot selection across mice were determined by matching investigation or hidebox epochs based on the duration of the event. Probability distribution curves were generated by plotting the kernel density

estimate of a cell's peak activity occurring ± 15 seconds of the corresponding hidebox of investigation event used for the heat maps.

Statistics

All statistical analyses were performed using Prism software (GraphPad). For comparison of two groups an unpaired Student's *t* test was used, except where noted. For comparison of multiple groups a one-way ANOVA was used, followed by Tukey's or Bonferroni's post hoc analysis. For comparison of two or more groups across treatment condition or time a two-way repeated measure ANOVA was used, followed by Bonferroni post-hoc analysis. Data distributions were tested for normality using the Kolmogorov-Smirnov normality test. If a dataset was not normally distributed, nonparametric analyses were applied. This is indicated where necessary in the manuscript. The sample sizes were determined based on those previously reported in studies related to our experimental assays[25,27,47].

Reporting Summary

Additional information regarding experimental design is available in the Nature Reporting Summary attached to this paper.

Supplementary Material

Refer to Web version on PubMed Central for supplementary material.

Acknowledgments

We thank Dr. Marta Soden for technical advice and assistance with slice electrophysiology, and members of the Zweifel lab for scientific discussion. We thank Dr. Carlos Campos, Anna Bowen and Dr. Richard Palmiter for their assistance with calcium imaging studies. We also thank Dr. James Allen for assistance in the production of AAV viral vectors. This work was funded by the US National Institutes of Health (P50MH10642 and R01MH094536 L.S.Z).

References

1. Elliot AJ The hierarchical model of approach-avoidance motivation. Motive Emotion 30, 111–116 (2006).
2. Choi GB et al. Lhx6 delineates a pathway mediating innate reproductive behaviors from the amygdala to the hypothalamus. Neuron 46, 647–660, doi:10.1016/j.neuron.2005.04.011 (2005). [PubMed: 15944132]
3. Burnett CJ et al. Hunger-Driven Motivational State Competition. Neuron 92, 187–201, doi:S0896–6273(16)30525–6 [pii] 10.1016/j.neuron.2016.08.032 (2016). [PubMed: 27693254]
4. Padilla SL et al. Agouti-related peptide neural circuits mediate adaptive behaviors in the starved state. Nature neuroscience 19, 734–741, doi:10.1038/nn.4274 (2016). [PubMed: 27019015]
5. Blanchard DC & Blanchard RJ Innate and conditioned reactions to threat in rats with amygdaloid lesions. J Comp Physiol Psychol 81, 281–290 (1972). [PubMed: 5084445]
6. Martinez RC, Carvalho-Netto EF, Ribeiro-Barbosa ER, Baldo MV & Canteras NS Amygdalar roles during exposure to a live predator and to a predator-associated context. Neuroscience 172, 314–328, doi:10.1016/j.neuroscience.2010.10.033 (2011). [PubMed: 20955766]
7. Olds ME & Olds J Approach-avoidance analysis of rat diencephalon. J Comp Neurol 120, 259–295 (1963). [PubMed: 13939939]

8. Dielenberg RA, Hunt GE & McGregor IS "When a rat smells a cat": the distribution of Fos immunoreactivity in rat brain following exposure to a predatory odor. Neuroscience 104, 1085–1097, doi:S0306452201001506 [pii] (2001). [PubMed: 11457592]
9. McGregor IS, Hargreaves GA, Apfelbach R & Hunt GE Neural correlates of cat odor-induced anxiety in rats: region-specific effects of the benzodiazepine midazolam. J Neurosci 24, 4134–4144, doi:10.1523/JNEUROSCI.0187-04.200424/17/4134 [pii] (2004). [PubMed: 15115808]
10. Chung AS, Miller SM, Sun Y, Xu X & Zweifel LS Sexual congruency in the connectome and translatome of VTA dopamine neurons. Scientific reports 7, 11120, doi:10.1038/s41598-017-11478-5 (2017). [PubMed: 28894175]
11. Bromberg-Martin ES, Matsumoto M & Hikosaka O Dopamine in motivational control: rewarding, aversive, and alerting. Neuron 68, 815–834, doi:10.1016/j.neuron.2010.11.022 (2010). [PubMed: 21144997]
12. Vincenz D, Wernecke KEA, Fendt M & Goldschmidt J Habenula and interpeduncular nucleus differentially modulate predator odor-induced innate fear behavior in rats. Behav Brain Res 332, 164–171, doi:S0166–4328(17)30294–2 [pii] 10.1016/j.bbr.2017.05.053 (2017). [PubMed: 28552601]
13. Ipser JC, Kariuki CM & Stein DJ Pharmacotherapy for social anxiety disorder: a systematic review. Expert Rev Neurother 8, 235–257, doi:10.1586/14737175.8.2.235 (2008). [PubMed: 18271710]
14. Garcia R Neurobiology of fear and specific phobias. Learn Mem 24, 462–471, doi:10.1101/lm.044115.11624/9/462 [pii] (2017). [PubMed: 28814472]
15. Dong HW, Petrovich GD & Swanson LW Topography of projections from amygdala to bed nuclei of the stria terminalis. Brain research. Brain research reviews 38, 192–246 (2001). [PubMed: 11750933]
16. Swanson LW The amygdala and its place in the cerebral hemisphere. Annals of the New York Academy of Sciences 985, 174–184 (2003). [PubMed: 12724158]
17. Gross CT & Canteras NS The many paths to fear. Nature reviews. Neuroscience 13, 651–658, doi:10.1038/nrn3301 (2012). [PubMed: 22850830]
18. Lein ES et al. Genome-wide atlas of gene expression in the adult mouse brain. Nature 445, 168–176, doi:nature05453 [pii] 10.1038/nature05453 (2007). [PubMed: 17151600]
19. Heusner CL, Beutler LR, Houser CR & Palmiter RD Deletion of GAD67 in dopamine receptor-1 expressing cells causes specific motor deficits. Genesis 46, 357–367, doi:10.1002/dvg.20405 (2008). [PubMed: 18615733]
20. Madisen L et al. A robust and high-throughput Cre reporting and characterization system for the whole mouse brain. Nat Neurosci 13, 133–140, doi:10.1038/nn.2467nn.2467 [pii] (2010). [PubMed: 20023653]
21. Zhang TY, Chretien P, Meaney MJ & Gratton A Influence of naturally occurring variations in maternal care on prepulse inhibition of acoustic startle and the medial prefrontal cortical dopamine response to stress in adult rats. J Neurosci 25, 1493–1502, doi:25/6/1493 [pii] 10.1523/JNEUROSCI.3293-04.2005 (2005). [PubMed: 15703403]
22. Unger EK et al. Medial amygdalar aromatase neurons regulate aggression in both sexes. Cell reports 10, 453–462, doi:10.1016/j.celrep.2014.12.040 (2015). [PubMed: 25620703]
23. Wang F et al. RNAscope: a novel in situ RNA analysis platform for formalin-fixed, paraffin-embedded tissues. The Journal of molecular diagnostics : JMD 14, 22–29, doi:10.1016/j.jmoldx.2011.08.002 (2012). [PubMed: 22166544]
24. Kollack-Walker S, Don C, Watson SJ & Akil H Differential expression of c-fos mRNA within neurocircuits of male hamsters exposed to acute or chronic defeat. J Neuroendocrinol 11, 547–559, doi:jne354 [pii] (1999). [PubMed: 10444312]
25. Lin D et al. Functional identification of an aggression locus in the mouse hypothalamus. Nature 470, 221–226, doi:10.1038/nature09736nature09736 [pii] (2011). [PubMed: 21307935]
26. Liu YX et al. Psychological stress on female mice diminishes the developmental potential of oocytes: a study using the predatory stress model. PloS one 7, e48083, doi:10.1371/journal.pone.0048083 (2012). [PubMed: 23118931]

27. Hong W, Kim DW & Anderson DJ Antagonistic control of social versus repetitive self-grooming behaviors by separable amygdala neuronal subsets. Cell 158, 1348–1361, doi:10.1016/j.cell.2014.07.049S0092-8674(14)01039-3 [pii] (2014). [PubMed: 25215491]
28. Choi JS & Kim JJ Amygdala regulates risk of predation in rats foraging in a dynamic fear environment. Proc Natl Acad Sci U S A 107, 21773–21777, doi:10.1073/pnas.1010079108 1010079108 [pii] (2010). [PubMed: 21115817]
29. Ghosh KK et al. Miniaturized integration of a fluorescence microscope. Nature methods 8, 871–878, doi:10.1038/nmeth.1694 (2011). [PubMed: 21909102]
30. Chen TW et al. Ultrasensitive fluorescent proteins for imaging neuronal activity. Nature 499, 295–300, doi:10.1038/nature12354 (2013). [PubMed: 23868258]
31. Pardo-Bellver C, Cadiz-Moretti B, Novejarque A, Martinez-Garcia F & Lanuza E Differential efferent projections of the anterior, posteroventral, and posterodorsal subdivisions of the medial amygdala in mice. Front Neuroanat 6, 33, doi:10.3389/fnana.2012.00033 (2012). [PubMed: 22933993]
32. Petrovich GD, Canteras NS & Swanson LW Combinatorial amygdalar inputs to hippocampal domains and hypothalamic behavior systems. Brain research. Brain research reviews 38, 247–289 (2001). [PubMed: 11750934]
33. Boyden ES, Zhang F, Bamberg E, Nagel G & Deisseroth K Millisecond-timescale, genetically targeted optical control of neural activity. Nature neuroscience 8, 1263–1268, doi:10.1038/nn1525 (2005). [PubMed: 16116447]
34. Blanchard RJ & Blanchard DC Attack and defense in rodents as ethoexperimental models for the study of emotion. Prog Neuropsychopharmacol Biol Psychiatry 13 Suppl, S3–14 (1989). [PubMed: 2694228]
35. Chuong AS et al. Noninvasive optical inhibition with a red-shifted microbial rhodopsin. Nature neuroscience 17, 1123–1129, doi:10.1038/nn.3752 (2014). [PubMed: 24997763]
36. Tervo DG et al. A Designer AAV Variant Permits Efficient Retrograde Access to Projection Neurons. Neuron 92, 372–382, doi:10.1016/j.neuron.2016.09.021 (2016). [PubMed: 27720486]
37. Flagel SB et al. A selective role for dopamine in stimulus-reward learning. Nature 469, 53–57, doi:10.1038/nature09588 (2011). [PubMed: 21150898]
38. Berridge KC & Robinson TE What is the role of dopamine in reward: hedonic impact, reward learning, or incentive salience? Brain research. Brain research reviews 28, 309–369 (1998). [PubMed: 9858756]
39. Dong HW & Swanson LW Projections from bed nuclei of the stria terminalis, posterior division: implications for cerebral hemisphere regulation of defensive and reproductive behaviors. The Journal of comparative neurology 471, 396–433, doi:10.1002/cne.20002 (2004). [PubMed: 15022261]
40. Marowsky A, Yanagawa Y, Obata K & Vogt KE A specialized subclass of interneurons mediates dopaminergic facilitation of amygdala function. Neuron 48, 1025–1037, doi:10.1016/j.neuron.2005.10.029 (2005). [PubMed: 16364905]
41. Schultz W Multiple dopamine functions at different time courses. Annual review of neuroscience 30, 259–288, doi:10.1146/annurev.neuro.28.061604.135722 (2007).
42. Pezze MA & Feldon J Mesolimbic dopaminergic pathways in fear conditioning. Progress in neurobiology 74, 301–320, doi:10.1016/j.pneurobio.2004.09.004 (2004). [PubMed: 15582224]
43. Yang H et al. Laterodorsal tegmentum interneuron subtypes oppositely regulate olfactory cue-induced innate fear. Nat Neurosci 19, 283–289, doi:10.1038/nn.4208nn.4208 [pii] (2016). [PubMed: 26727549]
44. Silva BA et al. Independent hypothalamic circuits for social and predator fear. Nat Neurosci 16, 1731–1733, doi:10.1038/nn.3573nn.3573 [pii] (2013). [PubMed: 24212674]
45. Hari Dass SA & Vyas A Copulation or sensory cues from the female augment Fos expression in arginine vasopressin neurons of the posterodorsal medial amygdala of male rats. Front Zool 11, 42, doi:10.1186/1742-9994-11-421742-9994-11-42 [pii] (2014). [PubMed: 24926317]
46. Bergan JF, Ben-Shaul Y & Dulac C Sex-specific processing of social cues in the medial amygdala. Elife 3, e02743, doi:10.7554/eLife.02743 (2014). [PubMed: 24894465]

47. Wang L, Chen IZ & Lin D Collateral pathways from the ventromedial hypothalamus mediate defensive behaviors. Neuron 85, 1344–1358, doi:10.1016/j.neuron.2014.12.025S0896-6273(14)01134-9 [pii] (2015). [PubMed: 25754823]
48. Golden SA et al. Persistent conditioned place preference to aggression experience in adult male sexually-experienced CD-1 mice. Genes Brain Behav 16, 44–55, doi:10.1111/gbb.12310 (2017). [PubMed: 27457669]
49. Ferrari PF, van Erp AM, Tornatzky W & Miczek KA Accumbal dopamine and serotonin in anticipation of the next aggressive episode in rats. Eur J Neurosci 17, 371–378, doi:2447 [pii] (2003). [PubMed: 12542674]
50. Couppis MH & Kennedy CH The rewarding effect of aggression is reduced by nucleus accumbens dopamine receptor antagonism in mice. Psychopharmacology (Berl) 197, 449–456, doi:10.1007/s00213-007-1054-y (2008). [PubMed: 18193405]
51. Zhuang X, Masson J, Gingrich JA, Rayport S & Hen R Targeted gene expression in dopamine and serotonin neurons of the mouse brain. J Neurosci Methods 143, 27–32, doi:S0165–0270(04)00350–4 [pii] 10.1016/j.jneumeth.2004.09.020 (2005). [PubMed: 15763133]
52. Gore BB & Zweifel LS Genetic reconstruction of dopamine D1 receptor signaling in the nucleus accumbens facilitates natural and drug reward responses. J Neurosci 33, 8640–8649, doi:10.1523/JNEUROSCI.5532-12.201333/20/8640 [pii] (2013). [PubMed: 23678109]
53. Sparta DR et al. Construction of implantable optical fibers for long-term optogenetic manipulation of neural circuits. Nat Protoc 7, 12–23, doi:10.1038/nprot.2011.413 (2012).
54. Resendez SL et al. Visualization of cortical, subcortical and deep brain neural circuit dynamics during naturalistic mammalian behavior with head-mounted microscopes and chronically implanted lenses. Nat Protoc 11, 566–597, doi:10.1038/nprot.2016.021nprot.2016.021 [pii] (2016). [PubMed: 26914316]
55. Sanz E et al. Fertility-regulating Kiss1 neurons arise from hypothalamic POMC-expressing progenitors. J Neurosci 35, 5549–5556, doi:10.1523/JNEUROSCI.3614-14.2015 (2015). [PubMed: 25855171]
56. Weber F et al. Control of REM sleep by ventral medulla GABAergic neurons. Nature 526, 435–438, doi:10.1038/nature14979 (2015). [PubMed: 26444238]
57. Kim JG et al. Leptin signaling in astrocytes regulates hypothalamic neuronal circuits and feeding. Nat Neurosci 17, 908–910, doi:10.1038/nn.3725 (2014). [PubMed: 24880214]
58. Chand AN, Galliano E, Chesters RA & Grubb MS A distinct subtype of dopaminergic interneuron displays inverted structural plasticity at the axon initial segment. J Neurosci 35, 1573–1590, doi:10.1523/JNEUROSCI.3515-14.2015 (2015). [PubMed: 25632134]
59. Ting JT, Daigle TL, Chen Q & Feng G Acute brain slice methods for adult and aging animals: application of targeted patch clamp analysis and optogenetics. Methods Mol Biol 1183, 221–242, doi:10.1007/978-1-4939-1096-0_14 (2014). [PubMed: 25023312]
60. Carter ME, Soden ME, Zweifel LS & Palmiter RD Genetic identification of a neural circuit that suppresses appetite. Nature 503, 111–114, doi:10.1038/nature12596 (2013). [PubMed: 24121436]
61. Soden ME et al. Genetic Isolation of Hypothalamic Neurons that Regulate Context-Specific Male Social Behavior. Cell Rep 16, 304–313, doi:10.1016/j.celrep.2016.05.067 (2016). [PubMed: 27346361]
62. Stamatakis AM & Stuber GD Activation of lateral habenula inputs to the ventral midbrain promotes behavioral avoidance. Nat Neurosci 15, 1105–1107, doi:10.1038/nn.3145 (2012). [PubMed: 22729176]
63. Zhou P et al. Efficient and accurate extraction of in vivo calcium signals from microendoscopic video data. Elife 7, doi:10.7554/eLife.28728e28728 [pii] 28728 [pii] (2018).
64. Pnevmatikakis EA et al. Simultaneous Denoising, Deconvolution, and Demixing of Calcium Imaging Data. Neuron 89, 285–299, doi:10.1016/j.neuron.2015.11.037S0896-6273(15)01084-3 [pii] (2016). [PubMed: 26774160]
65. Jimenez JC et al. Anxiety Cells in a Hippocampal-Hypothalamic Circuit. Neuron 97, 670–683 e676, doi:S0896–6273(18)30019–9 [pii] 10.1016/j.neuron.2018.01.016 (2018). [PubMed: 29397273]

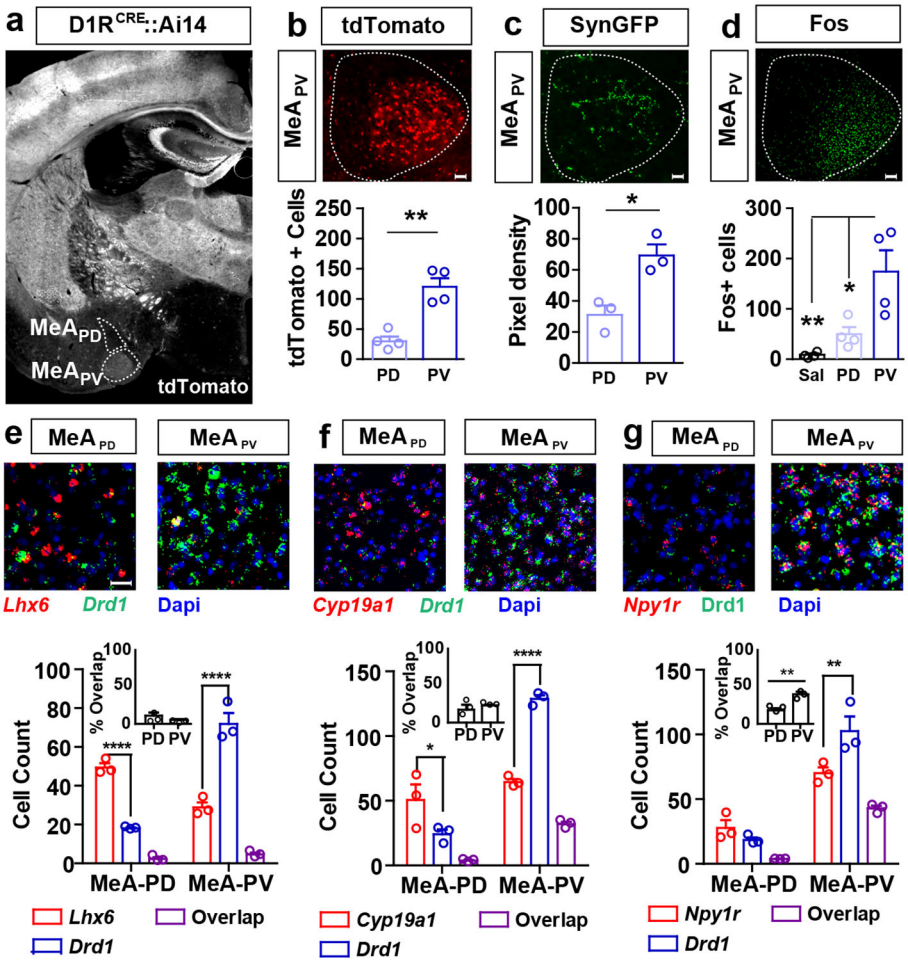

Figure 1.

Identification of dopamine receptive neurons in the MeApv. (a) Coronal section of D1R-Cre::Ai14 reporter mouse showing localization of tdTomato expressing *Drd1* neurons in the MeApv. This was replicated in three other mice. (b) (Top) High-magnification image of D1R:tdTomato cells; (Below) quantification showing more TdTmto-positive cells in MEApv versus MeApd (n=4 mice, **P=0.0014, two-tailed unpaired *t* test). Scale bar: 50 μm. Center values represent mean, error bars represent s.e.m. (c) (Top) Projections of midbrain DAT neurons revealed by expression of syn-GFP in axon terminals in the MeApv; (Below) quantification of projections showing denser projections to MeApv vs. MeApd (n=3 mice, *P=0.0165, two-tailed unpaired *t* test). Scale bar: 50 μm. Center values represent mean, error bars represent s.e.m. (d) (Top) Immunohistochemistry of MeApv following i.p. injection of SKF 81, 297 (7.5 mg/kg) showing increased Fos induction; (Below) quantification of Fos demonstrates a significantly higher Fos induction in the MeApv compared to the MeApd (n=4 mice/group; 1-way ANOVA $F_{(2, 9)} = 11.09$, P=0.0037, two-tailed Tukey's multiple comparisons test **P=0.0081, *P=0.032). Scale bar: 100 μm. Center values represent mean, error bars represent s.e.m. (e-g) Top: Single-molecule fluorescence *in situ* for *Drd1* (green) and indicated alternate cell markers (red) in MeApd and MeApv. Below: Quantification of fluorescent cells confirming that majority of Drd1-expressing neurons are located in the MeApv. Insets: % of Drd1 cells that also express indicated market demonstrating minimal

overlap between *Drd1* and *Lhx6* or *Cyp19a1*, and modest overlap with *Npy1r* (n=3 mice/group, 2-way ANOVA, two-tailed Bonferroni's multiple comparisons test, *Lhx6*: $F_{(2, 8)}$ = 85.13, ****P<0.0001; *Cyp19a1*: $F_{(2, 6)}$ = 30.92, *P=0.045, ****P<0.0001; *Nyp1r*: $F_{(2, 8)}$ = 18.81, P=0065; Inset of *Nyp1r*: P=0.0082, two-tailed unpaired *t* test). Scale bar: 30 μm. Center values represent mean, error bars represent s.e.m.

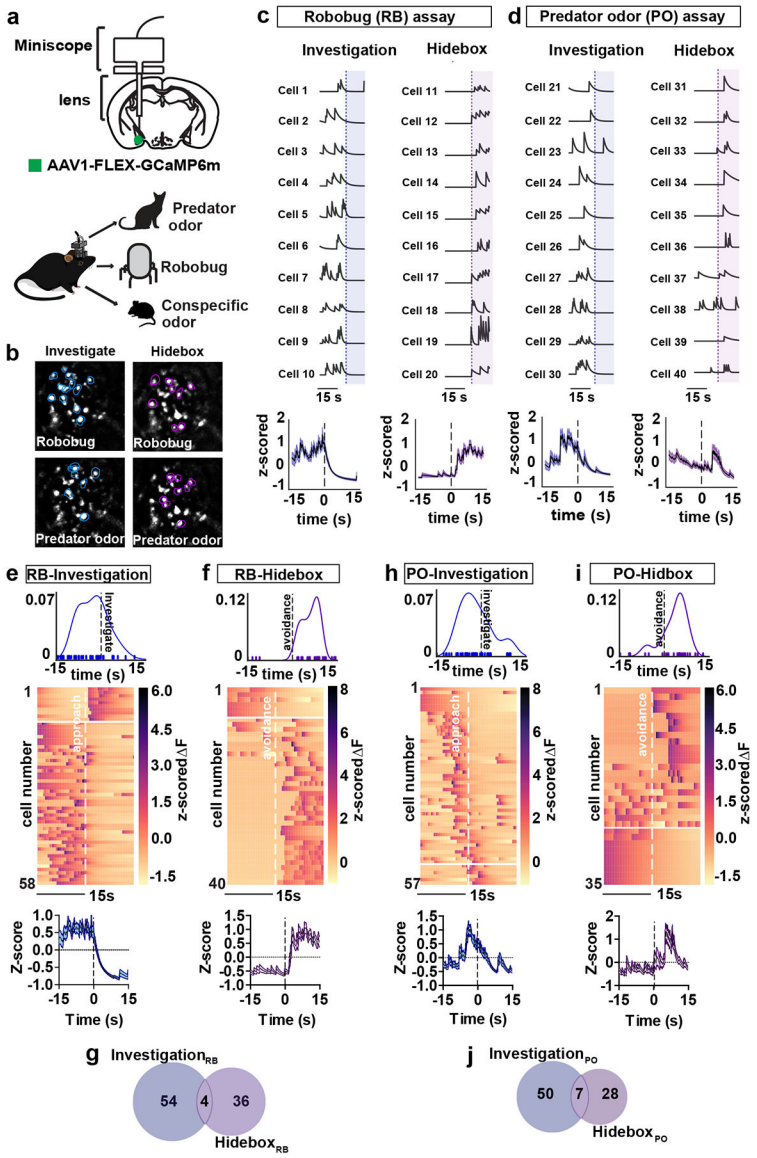

Figure 2.

MeApv-D1R neurons are activated during approach and avoidance to predator odor and robobug. (a) Schematic of miniscope, lens and viral injection for calcium imaging and behavior. (b) Field-of-view (FOV) of MeApv D1R::GCaMP6m neurons from each of the four designated behavioral epochs. Open circles represent designated regions of interest (ROI) from a subset of cells categorized as active during the behavioral epoch. (c-d) Top: single traces of a subset of cells activated during approach or hidebox (n= one mouse). Bottom: average of the cells presented above (n=10 cells/behavioral epoch from one mouse). (e) Activity profiles of cells from all mice during robobug investigation (n= 4 mice). Top: probability of distribution of peak fluorescence for all cells active during approach to robobug (dashed line represents initiation of investigation, n=58 cells from 4 mice); Middle: heat plot of calcium responses during an approach and investigation epoch for all active cells (n=58 cells from 4 mice); Bottom: average traces of all cells activated prior to an approach

and investigation epoch ± shaded areas represent s.e.m. (n = 58 cells from 4 mice). (f) Activity profiles of cells from all mice during hidebox period from robobug assay. Top: probability of distribution of peak fluorescence for all cells active following entry into hidebox (dashed line represents entry into hidebox, n= 40 cells from 4 mice); Middle: heat plot of calcium responses following entry into hidebox for all the active cells aligned to a hidebox entry (n=40 cells from 4 mice); Bottom: average traces of all cells activated following an entry to the hidebox ± shaded areas represent s.e.m. (n = 40 cells from 4 mice) (g) Selectivity of cells active during robobug assay (n=4 mice). (h-i) Same as (e-g) for predator odor assay. For approach and investigation behavior: n=57 cells from 4 mice. For hide box behavior: n=35 cells from 4 mice. Shaded areas represent s.e.m. (j) Selectivity of cells active during predator odor assay (n=4 mice).

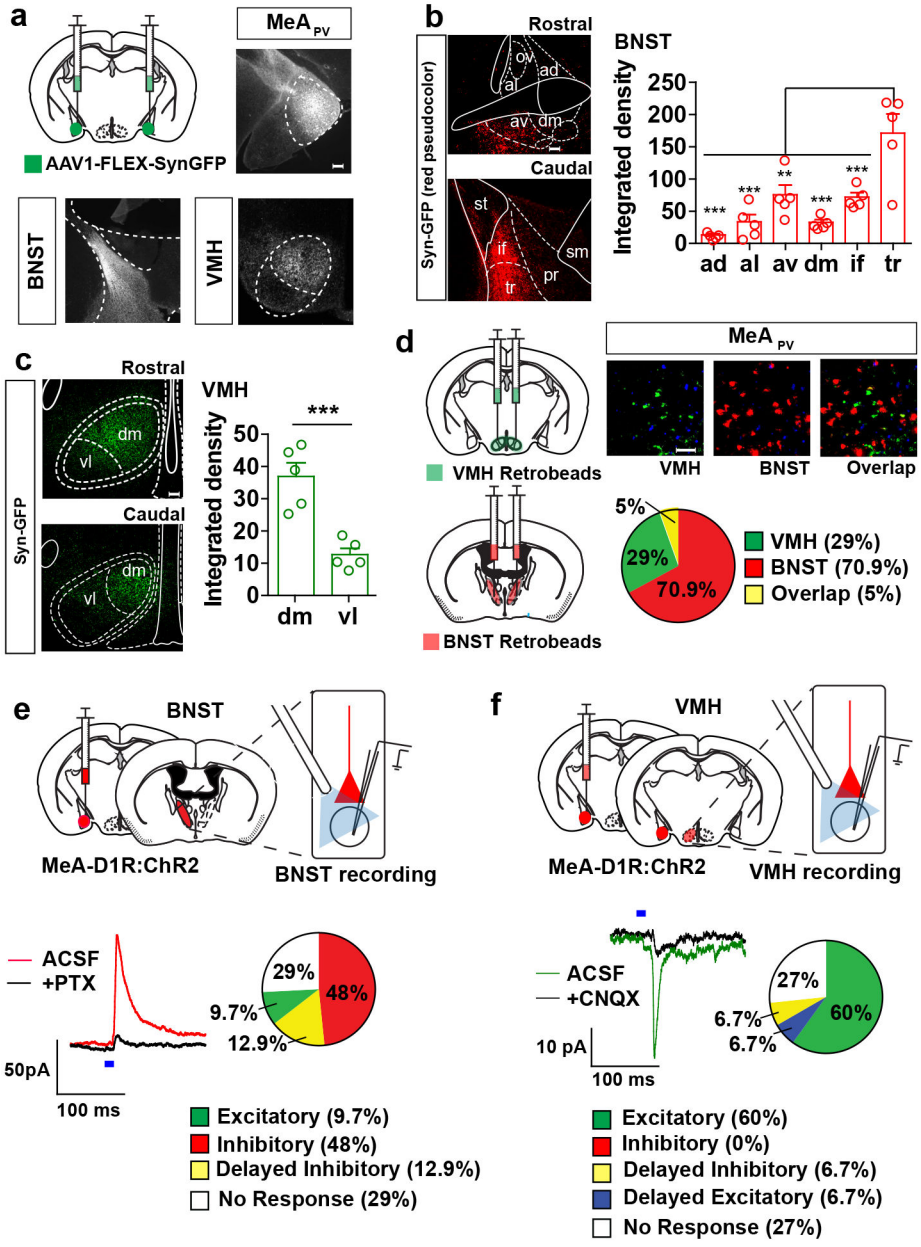

Figure 3.

Anatomical and synaptic connectivity of MeApv-D1R neurons. (a) Schematic of bilateral viral injection of AAV1-FLEX-syn-GFP into MeApv of a D1R-Cre mouse. Histology showing cell body expression of syn-GFP in MeApv D1R neurons, and revealing projections of MeApv D1R neurons in BNST and VMHdm. Scale bar: 50 μm. (b) Detailed synaptophysin mapping showing fiber density of MeApv D1R neuron projections within sub-regions of BNST, with dense fibers in the transverse nucleus of BNST (n=5 mices, 1-way ANOVA $F_{(5, 24)} = 14.81$, $P<0.0001$, Tukey's multiple comparisons test, ad vs tr: P=0.0002; al vs. tr: P= 0.00025; av vs. tr: P= 0.0025; dm vs. tr: P= 0.00017; if vs. tr: P= 0.00012) and (c) fibers in sub-regions of VMH, with dense fibers in the dorsomedial VMH (n=5 mice, P=0.0009, two-tailed unpaired *t* test). Scale bar: 50 μm. Center values represent

mean, error bars represent s.e.m. (d) Schematic showing injection of green RetroBeads injected into the VMH and red RetroBeads injected into the BNST. Significantly more MeApv neurons are labeled by BNST injections and there is very little overlap of green and red beads (70.9% red; 29% green; 5% overlap; n=3 mice; $P<0.0001$, *Chi* squared). Scale bar: 30 μm. (e) Schematic showing whole cell patch preparation in which ChR2-mCherry is transduced into the MeApv of D1R-Cre mice and whole cell patch recordings are made in BNST. Example trace of a blue light-evoked IPSC in the BNST (holding at 0 mV); the IPSC could be blocked by bath application of PTX (100 μM). Each trace is an average of 30 sweeps. Pie chart shows distribution of responses recorded in BNST (n=31 cells/5 mice). (f) Schematic showing whole cell patch preparation in which ChR2-mCherry is transduced into the MeApv of D1R-Cre mice and whole cell patch recordings are made in VMHdm. Example trace of blue light-evoked EPSC in the VMHdm (holding at −60 mV); the EPSC could be blocked by bath application of CNQX (10 μM). Each trace is an average of 30 sweeps. Pie chart shows distribution of responses recorded in VMH. (n=15 cells/4 mice).

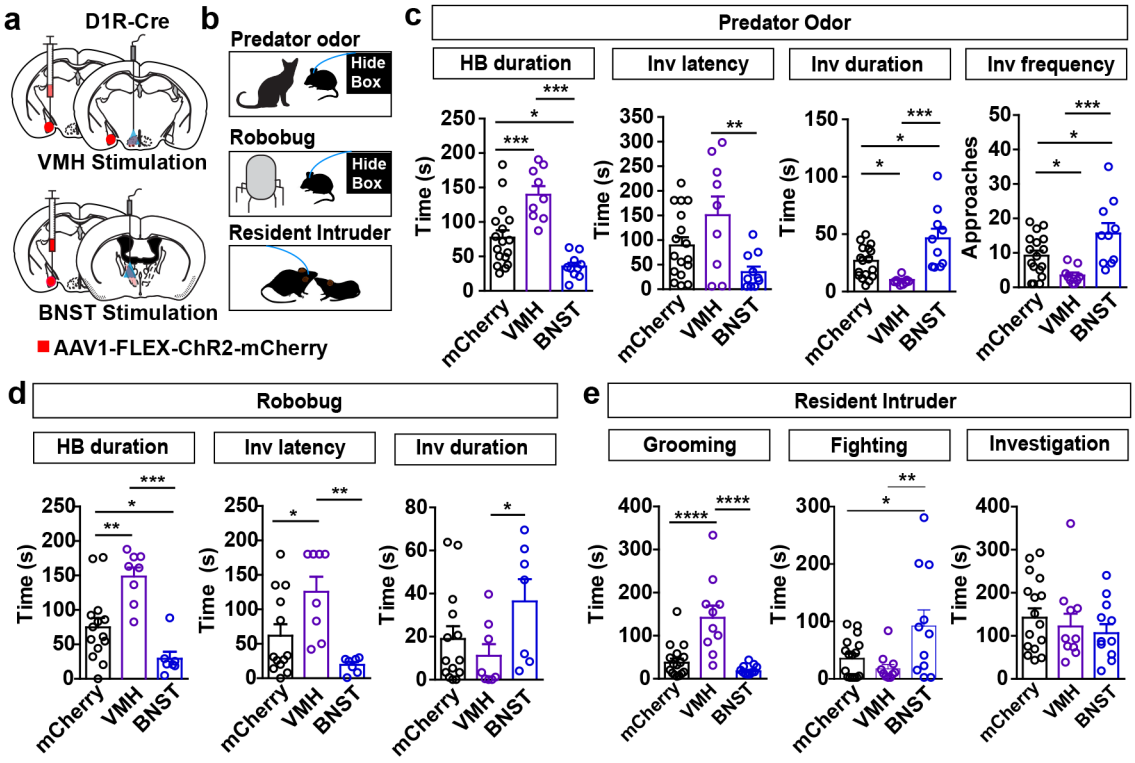

Figure 4.

Activation of distinct MeApv-D1R pathways differentially drives approach and avoidance. (a-b) Schematic of viral injection of AAV1-FLEX-ChR2-mCherry, fiber-optic implant, and behavioral paradigms for threat exposure. (c) Optogenetic activation of VMH-projecting MeApv-D1R neurons increases avoidance of predator odor, while optogenetic activation of BNST-projecting MeApv D1R neurons increases approach to predator odor (n=17, 9, 10 mice/group; Time spent in hide box: 1-way ANOVA $F_{(2, 33)} = 19.18$, P<0.0001; Latency to approach: 1-way ANOVA $F_{(2, 33)} = 5.501$, P=0.0087; Investigation time: 1-way ANOVA $F_{(2, 33)} = 11.1$, P=0.0002; Frequency of investigations: 1-way ANOVA $F_{(2, 33)} = 7.949$, P=0.0015). (d) Optogenetic activation of VMH-projecting MeApv-D1R neurons increases avoidance of robobug. Optogenetic activation of BNST-projecting MeApv-D1R neurons increases approach to robobug (n=17, 9, 10 mice; Time spent in hide box: 1-way ANOVA Kruskal-Wallis with Dunn's multiple comparison P=0.0007; Latency to approach: 1-way ANOVA Kruskal-Wallis with Dunn's multiple comparison P=0.0039; Investigation time: 1-way ANOVA $F_{(2, 26)} = 2.607$, P=0.0929). (e) Optogenetic activation of VMH-projecting MeApv-D1R neurons increases grooming of conspecific during resident-intruder assay and optogenetic activation of BNST-projecting MeApv-D1R neurons increases fighting of conspecific during resident-intruder assay (n=16, 10, 11 mice/group; grooming: 1-way ANOVA $F_{(2, 31)}= 16.88$, P<0.0001; fighting: 1-way ANOVA $F_{(2, 31)}= 5.048$, P=0.012; investigation: 1-way ANOVA $F_{(2, 31)}= 0.6207$, P=0.5435). Unless otherwise indicated, for all panels Tukey's multiple comparisons test was used, For all, center values represent mean, error bars represent s.e.m.

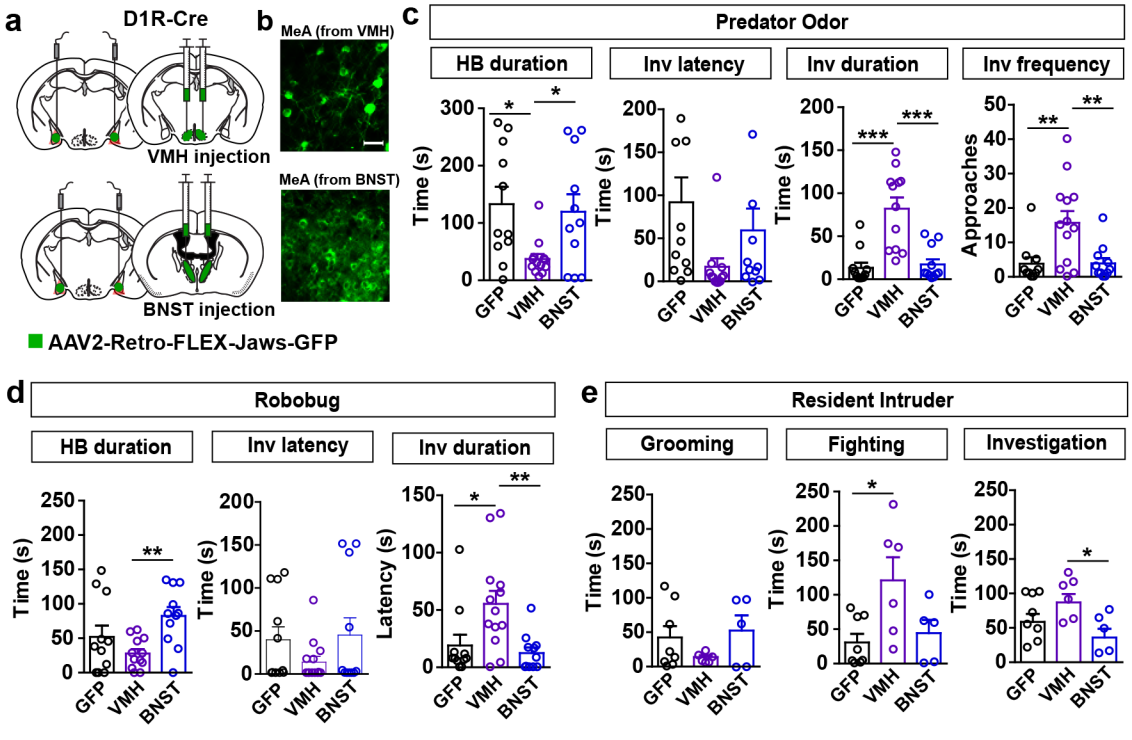

Figure 5.

Inhibition of distinct MeApv-D1R pathways differentially drives approach and avoidance. (a) Schematic of viral injection of AAV2-Retro-FLEX-JAWS-GFP, fiber-optic implant. (b) Histology showing MeApv-D1R cell bodies transfected with JAWS-GFP from injection in VMH (top) and BNST (bottom). Scale bar: 15 μm. This was replicated in 12 mice for the VMH and 10 mice for the BNST. (c) Optogenetic inhibition of VMH-projecting MeApv-D1R neurons increases approach to predator odor. Optogenetic inhibition of BNST-projecting MeApv-D1R neurons does not alter response to predator odor (n=11, 12, 10 mice/group; Time spent in hide box: 1-way ANOVA $F_{(2, 35)}$ = 4.945, P=0.0134; Latency to approach: 1-way ANOVA Kruskal-Wallis with Dunn's multiple comparison P=0.01707; Investigation time: 1-way ANOVA Kruskal-Wallis with Dunn's multiple comparison P=0.003; 1-way ANOVA Kruskal-Wallis with Dunn's multiple comparison P=0.0175). (d) Optogenetic inhibition of VMH-projecting MeApv-D1R neurons increases approach to robobug. Optogenetic inhibition of BNST-projecting MeApv D1R neurons does not alter response to robobug (n=11, 12, 10 mice/group; Time spent in hide box: 1-way ANOVA $F_{(2, 31)}$ = 4.966, P=0.0135; Latency to approach stimulus: 1-way ANOVA Kruskal-Wallis with Dunn's multiple comparison P=0.3045; Investigation time: 1-way ANOVA Kruskal-Wallis with Dunn's multiple comparison P=0.0091). (e) Optogenetic inhibition of VMH-projecting MeApv-D1R neurons enhances of righting toward conspecific during resident-intruder assay and optogenetic inhibition of BNST-projecting MeApv D1R neurons does not affect social behavior during resident-intruder assay (n=8, 6, 5 mice/group; grooming: 1-way ANOVA $F_{(2, 16)}$ = 1.466, P=0.2603; fighting: 1-way ANOVA $F_{(2, 16)}$= 4.85, P=0.0226; Investigation: 1-way ANOVA $F_{(2, 16)}$= 3.765, P=0.0448). Unless otherwise indicated, for all panels Tukey's multiple comparisons test was used. For all, center values represent mean, error bars represent s.e.m.

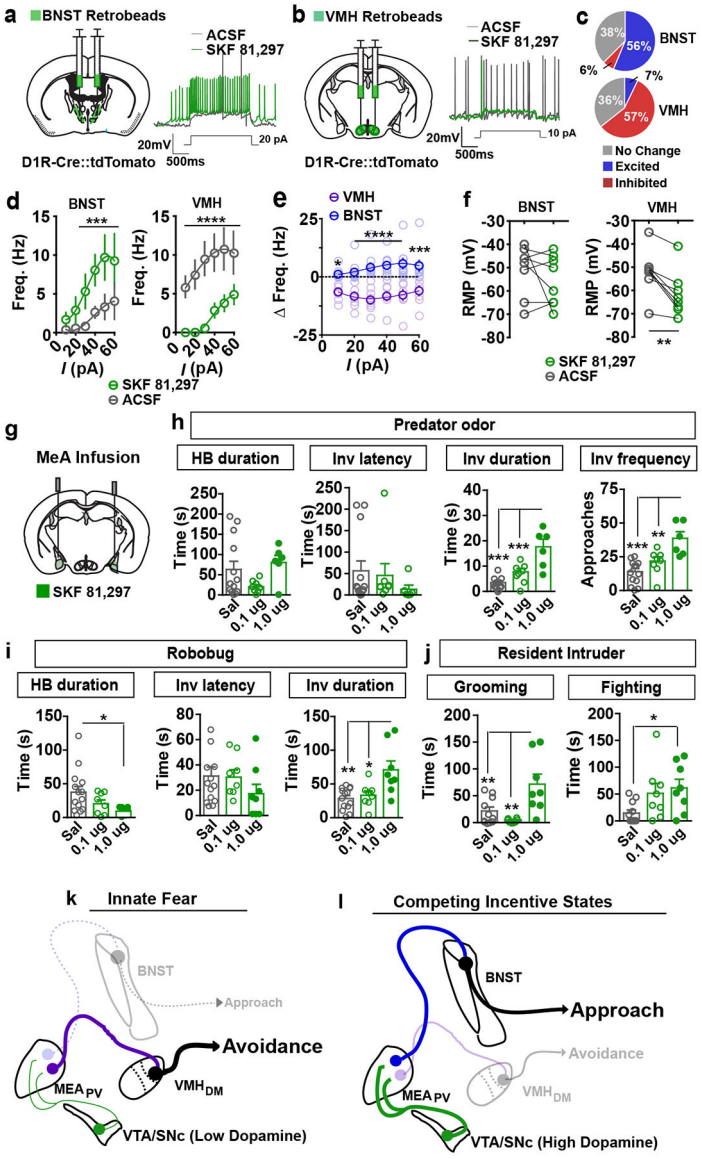

Figure 6.

D1R signaling biases activation of MeA→BNST approach pathway. Schematic of retrobead injection into (a) BNST and (b) VMH of D1R-Cre::tdTomato mice and representative traces showing action potential firing before (ACSF) and after bath application of SKF 81,297 (10 μM). (c) Distribution of cells that were excited (BNST n=9 out 16 cells; VMH n=1 out of 14 cells), inhibited (BNST n=1 out of 16 cells; VMH n=8 out of 14 cells) or non-responsive (BNST n=6 out of 16 cells; VMH n=5 out of 14 cells) to SKF 81,297. (d) Quantification of spike frequency from responsive cells shows increased spiking frequency in response to current step injections following application of SKF 81,297 in BNST projecting MeApv-D1R neurons (n=9 cells/3 mice, 2-way ANOVA, effect of drug, $F_{(5, 60)}$= 8.581, P<0.0001) and decreased spiking frequency in VMH projecting MeApv-D1R neurons (n=8 cells/3 mice, 2-way ANOVA, effect of drug, $F_{(5, 65)}$= 7.831, P<0.0001). (e) Comparison of change in spiking (ΔAP number) before and after SKF 81,297 application showing increase in

BNST relative to VMH projecting MeApv-D1R neurons (n=17 cells/6 mice, 2-way ANOVA, $F_{(5, 75)}$= 5.124, P=0.0004). (f) Resting membrane potential (RMP) was not different before and after SKF 81, 297 application in BNST projecting MeApv-D1R cells but was hyperpolarized in VMH projecting MeApv-D1R cells (n=9 cells/3 mice, 8 cells/3 mice, P=0.0039, two-tailed paired *t* test). (g) Schematic of bilateral microinfusion of D1R agonist SKF 81, 297 (low dose: 0.1μg/0.5μl per side; high dose: 1μg/0.5μl per hemisphere) locally into the MEA. (h) Infusion of SKF 81,297 increased approach to predator odor in dose dependent manner (n=14, 8, 8 mice/group; Time spent in hide box: 1-way ANOVA Kruskal-Wallis with Dunn's multiple comparison P=0.212; Latency to approach: 1-way ANOVA Kruskal-Wallis with Dunn's multiple comparison P=0.1384; Investigation time: 1-way ANOVA $F_{(2, 24)}$ = 5.083, P=0.0144; Frequency of investigations: 1-way ANOVA $F_{(2, 24)}$ = 13.56, P=0.0001). (i) Infusion of SKF 81,297 dose-dependently increased approach to robobug (n=14, 8, 8 mice/group; Time spent in hide box: 1-way ANOVA $F_{(2, 27)}$ = 3.72, P=0.0374; Latency to approach: 1-way ANOVA $F_{(2, 27)}$ = 1.037, P=0.3683; Investigation time: 1-way ANOVA $F_{(2, 27)}$ = 8.776, P=0.0012). (j) Infusion of increasing doses of SKF 81,297 increased fighting dose-dependently during resident-intruder assay but has no effect on grooming behavior (n=11, 8, 8 mice/group; grooming: 1-way ANOVA $F_{(2, 24)}$ = 9.12, P=0.0011; fighting: 1-way ANOVA Kruskal-Wallis with Dunn's multiple comparison P=0.0262). (k-i) Proposed model for how competing incentive states modulate VMH versus BNST MEA_{PV}-D1R pathways depending on dopamine levels in the amygdala. Under low competing incentive states when dopamine levels are low the MEApv-D1R→ VMH pathway predominates to mediate avoidance. Under high competing incentive states when dopamine levels are increased the MEApv-D1R→BNST predominates to mediate approach in the face of danger. Unless otherwise indicated, Tukey's multiple comparisons test used for a 1-way ANOVA and Bonferonni's multiple comparison's test was used for 2-way ANOVA. For all, center values represent mean, error bars represent s.e.m.